A regular Hamiltonian halting ratchet for matter wave transport

N. Dupont,[1,2] L. Gabardos,[1] F. Arrouas,[1] N. Ombredane,[1] J. Billy,[1] B. Peaudecerf,[1] and D. Guéry-Odelin[1]

[1] *Laboratoire Collisions Agrégats Réactivité, UMR 5589, FERMI, UT3, Université de Toulouse, CNRS, 118 Route de Narbonne, 31062 Toulouse CEDEX 09, France*

[2] *Center for Nonlinear Phenomena and Complex Systems, Université Libre de Bruxelles, CP 231, Campus Plaine, B-1050 Brussels, Belgium*

(Dated: April 5, 2023)

We report on the design of a Hamiltonian ratchet exploiting periodically at rest integrable trajectories in the phase space of a modulated periodic potential, leading to the linear non-diffusive transport of particles. Using Bose-Einstein condensates in a modulated one-dimensional optical lattice, we make the first observations of this new spatial ratchet transport. In the semiclassical regime, the quantum transport strongly depends on the effective Planck constant due to Floquet state mixing. We also demonstrate the interest of quantum optimal control for efficient initial state preparation into the transporting Floquet states to enhance the transport periodicity.

The ratchet effect is the well-known yet intriguing phenomenon which sees the emergence of a directed current for particles initially at rest in a space and time periodic modulated potential, while no net average force is exerted on the system. Its origin is well understood and relies minimally on the breaking of space and time reversal symmetries [1–3]. Two main families of ratchets can be distinguished: on one hand, *Brownian ratchets* are systems experiencing stochastic forces, where the potential rectifies the isotropy of Brownian motion [4] into a net directed transport [5–7]. Such ratchets are thought to take part in the operation of molecular motors [8, 9], as for instance in the case of kinesin [10]. They are usually studied in the overdamped regime to model the strong dissipation of biological media [7, 11]. On the other hand, *deterministic ratchets*, which can be either dissipative [1, 12–19] or Hamiltonian (see below), are systems for which the classical dynamics is well captured by their phase space flow. Such Hamiltonian systems, under moderate temporal driving, exhibit a mixed dynamics with phase portraits displaying islands of regular trajectories embedded in a chaotic sea of non-integrable ones (see e.g. Fig. 1).

Studies on Hamiltonian ratchets have mainly focused thus far on delocalized transport configurations, where the directed transport originates in a momentum-asymmetric chaotic sea: in the classical case from trajectories ergodically spanning the chaotic sea [1, 14, 20], and in the quantum case through state coupling with eigenstates delocalized over it [20–23]. In contrast, Hamiltonian ratchets relying on regular islands of quasi-periodic trajectories offer a mean to incrementally transport localized particles on a periodic substrate in a ballistic way [21]. Note that this transport appears classically and is distinct from topological pumping effects ([24] and references therein). Such regular Hamiltonian ratchets have been experimentally studied mainly with phase-shifted kicked-rotors, implemented in cold atom systems, in the case of step-wise transport along the momentum direction (an *accelerator ratchet*) [25–27], and with only up to 20% of an initial atom packet loaded in the transporting island. Meanwhile, regular Hamiltonian ratchets along the position coordinate [28] remain unexplored experimentally so far. Beyond the use of regular islands with a ballistic motion at all times, as found e.g. in the kicked rotor, of particular interest is the design of a dynamical system in which the transporting island periodically coincides with the ground state of the potential, in which a collection of particles initially at rest can therefore be directly loaded and transported.

In this Letter, we solve this non-trivial problem, the solution of which we refer to as a *spatial halting ratchet* (SHR). We show how such a solution can be engineered with a simple gating ratchet [18, 29], a one-dimensional space-symmetric potential modulated in amplitude and phase. We obtain parameters leading to classical orbits of initial zero velocity having a ratcheting motion of one spatial period per modulation period. For these parameters, we study quantum transport as a function of the effective reduced Planck constant $\hbar_{\text{eff}}$, which sets the minimal phase-space area of quantum states. As a modulation parameter such as $\hbar_{\text{eff}}$ is varied, avoided crossings in the Floquet spectrum lead to state mixing. Although this phenomenon is sought after in the case of diffusive Hamiltonian ratchets [22, 30] where it is the source of transport, and is also key in chaos-assisted tunneling [31, 32], it has a deleterious effect in the regular transport case, as a wave packet initially prepared over the classical ratcheting island may dynamically tunnel [33] out of it. This may be avoided by a precise choice of parameter values, or controlled through specific state preparation. From our theoretical analysis, we implement and observe experimentally the SHR with matter waves, using Bose-Einstein condensates (BECs) in a modulated one-dimensional optical lattice. We first perform these experiments by loading the ratcheting Floquet state from the ground state of the lattice. For values of $\hbar_{\text{eff}}$ for which the ratcheting island is substantially coupled with the chaotic sea, we then show how one can account for state mixing by employing quantum optimal

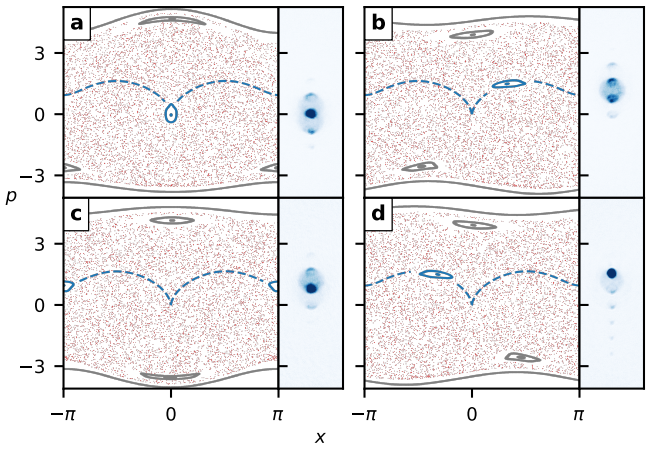

FIG. 1. **Stroboscopic phase portraits and experimental images** for $(\gamma, \varepsilon, \varphi_0) = (1.2, 0.3, 1.7)$ at sub-period observation times $t = (n + r) \times 2\pi$ (with $n \in \mathbb{N}$ and $r = 0$, 0.25, 0.5 and 0.75 for **(a)** to **(d)** resp.). Left: the ratcheting island and the trajectory starting in $(x_0, p_0, t_0) = (0, 0, 0)$ are in blue, the other regular structures are in gray and the chaotic sea is in red. The area of the ratcheting island is $\mathcal{A} = 0.21$. Right: corresponding time-of-flight absorption images, starting from the ground state of the lattice during the first period $n = 0$ for $1/\hbar_{\text{eff}} \approx 1.27$.

control (QOC) [34, 35] to optimize the loading of the proper Floquet state.

Classical dynamics. We consider the case of an inertial particle in a gating potential [18, 29]. Its dynamics is governed by the dimensionless Hamiltonian

$$H(x, p, t) = \frac{p^2}{2} - \gamma \left[1 + \varepsilon \cos(t)\right] \cos\left[x - \varphi_0 \sin(t)\right]. \quad (1)$$

The Hamiltonian of Eq. (1), with its 1:1 frequency ratio and phase quadrature between amplitude and phase modulations, breaks the relevant space and time symmetries [1, 18], leading to a momentum-asymmetric chaotic sea carrying diffusive ratchet transport. In contrast, the dimensionless modulation parameters $(\gamma, \varepsilon, \varphi_0)$ can also be chosen so that a transporting regular region emerges in the center of the chaotic sea, *i.e.* such that a bundle of trajectories starting around $(x_0, p_0) = (0, 0)$ at $t_0 = 0$ goes to the neighborhood of $(x_0 + 2\pi, p_0)$ at $t = 2\pi$. We achieve this numerically by minimizing with respect to $(\gamma, \varepsilon, \varphi_0)$ (using a Nelder-Mead algorithm) the total variation of mechanical energy over one modulation period for a set of trajectories that start near (x_0, p_0) and change site. This yields several solutions [36]. In the following we use $(\gamma, \varepsilon, \varphi_0) = (1.2, 0.3, 1.7)$, a set of parameters that generates a SHR with the ratcheting island seen in the stroboscopic phase portraits of Fig. 1.

Quantum ratchet in a regular island. The natural basis to stroboscopically study quantum dynamics in a time-periodic potential is the set of Floquet states, the eigenstates of the evolution operator over one period of modulation. The quantum study leaves as a free parameter the effective reduced Planck constant $\hbar_{\text{eff}} = -i[\hat{x}, \hat{p}]$ that dictates the minimal phase-space area $\Delta x \Delta p$ of quantum states in the system. As we are interested in the transport of a quantum particle on the ratcheting island, we place our study at the onset of the semiclassical regime, that is for $\hbar_{\text{eff}} \sim \mathcal{A}$, with $\mathcal{A}$ the area of the studied regular structures in phase space (Fig. 1). In the semiclassical regime, Floquet states are generally either localized on regular islands or spread over the chaotic sea [37, 38], with only one state per island for $\hbar_{\text{eff}} \sim \mathcal{A}$. The quantum analogue of the periodic classical trajectories at the center of the stroboscopic phase portraits of Fig. 1(a) is therefore the Floquet state $|\mathrm{F_{rat}}\rangle$ that can be associated with the ratcheting island. This state is identified from its overlap with the ground state $|\phi_0\rangle$ of the static lattice potential (that is $\varepsilon = 0$ and $\varphi_0 = 0$ in Eq. (1) ; a state readily accessible in the experiment). Furthermore, we define the expected transport of a state $|\psi(t_0)\rangle$ between the times t_0 and t_1 as

$$\Delta x_{(t_0,t_1)}(\psi) = \int_{t_0}^{t_1} \langle \hat{p} \rangle_{\psi(t)} \, dt. \quad (2)$$

The transport over one period $\Delta x_{(0,2\pi)}(\mathrm{F})$ for a Floquet state $|\mathrm{F}\rangle$ is related to its time-averaged group velocity $\overline{v}_g$ in the Floquet spectrum, $\Delta x_{(0,2\pi)}(\mathrm{F}) = 2\pi \overline{v}_g$ (see Supplemental Material). In the semiclassical regime, one expects regular Floquet states to behave as their associated region of regular classical trajectories, and, in particular for the ratcheting Floquet state, $\Delta x_{(0,2\pi)}(\mathrm{F_{rat}}) \approx 2\pi$.

We illustrate these notions in Fig. 2 where numerical results for the transport of non-interacting wave functions in the ratcheting island as a function of $1/\hbar_{\text{eff}}$ are shown. Figure 2(a) shows the overlap between $|\mathrm{F_{rat}}\rangle$ and the ground state $|\phi_0\rangle$. This metric informs on the phase-space centering of $|\mathrm{F_{rat}}\rangle$, as well as on its expected loading when running the experiment with $|\phi_0\rangle$ as the initial state. Figure 2(b) shows the expected periodic transport of $|\mathrm{F_{rat}}\rangle$. As $1/\hbar_{\text{eff}}$ varies, both $|\langle\phi_0|\mathrm{F_{rat}}\rangle|^2$ and $\Delta x_{(0,2\pi)}(\mathrm{F_{rat}})$ (Fig. 2(a) and (b) resp.) display sharp non-monotonic fluctuations ascribed to Floquet state mixing: the variation of quasi-energy levels in the Floquet spectrum gives rise to avoided crossings leading to sharp changes of the Floquet states near the crossings (see Supplemental Material).

Figures 2(c-e) shows the Husimi quasi-distributions of $|\phi_0\rangle$ and $|\mathrm{F_{rat}}\rangle$ for different values of $1/\hbar_{\text{eff}}$. With $1/\hbar_{\text{eff}} = 1.27$, Fig. 2(d) is an example of a semiclassical, island-shaped $|\mathrm{F_{rat}}\rangle$, with a ground state overlap $|\langle\phi_0|\mathrm{F_{rat}}\rangle|^2 = 0.86$ and a periodic transport $\Delta x_{(0,2\pi)}(\mathrm{F_{rat}}) = 0.93 \times 2\pi$, meaning that this state exhibits a stationary flux of particles, periodically at rest at the bottom of the lattice wells. On the other hand, Fig. 2(c) and (e) correspond to respectively smaller and larger values of $1/\hbar_{\text{eff}}$ for which

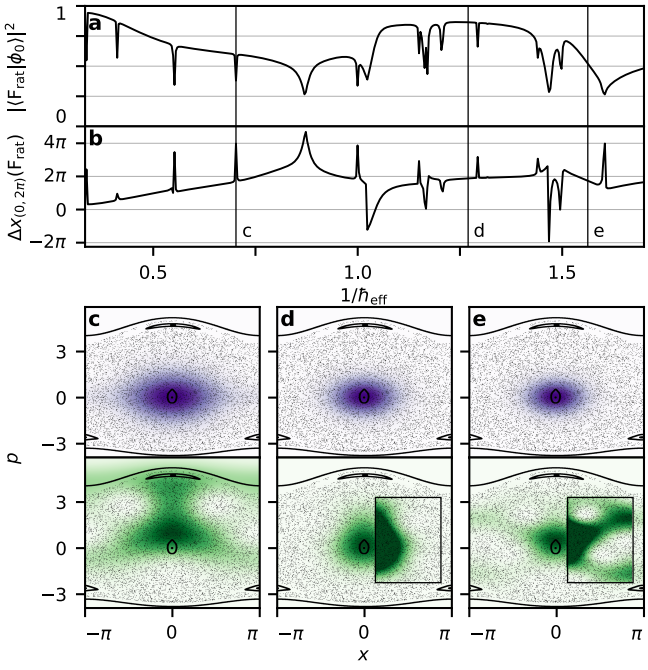

FIG. 2. **Eigenstate and transport dependences on the effective Planck constant. (a)** Overlap between the ground state $|\phi_0\rangle$ of the lattice and the ratcheting Floquet state $|\mathrm{F_{rat}}\rangle$ and **(b)** transport (2) of $|\mathrm{F_{rat}}\rangle$ over one modulation period as a function of $1/\hbar_{\mathrm{eff}}$. **(c-e)** Stroboscopic phase portraits in the unit cell of system (1) and Husimi representations of $|\phi_0\rangle$ (top, purple) and $|\mathrm{F_{rat}}\rangle$ (bottom, green) for the values of $1/\hbar_{\mathrm{eff}} = 0.70, 1.27, 1.56$ respectively, identified by vertical lines on the panels (a-b). The color range for each Husimi function extends from zero to its maximum value, with a truncation to a quarter of this value in the inset of panels (d,e) in order to reveal details.

the system initialized in $|\phi_0\rangle$ evolves out of it (towards a mode of high momentum for Fig. 2(c) and over the chaotic sea for Fig. 2(e)). Figure 2 shows overall that, for sufficiently large values of $1/\hbar_{\mathrm{eff}}$ and while paying attention to Floquet state mixing, a SHR with a semiclassical periodic transport of quantum states can be achieved, with $\Delta x_{(0,2\pi)}(\mathrm{F_{rat}})$ fluctuating around 2π for $1/\hbar_{\mathrm{eff}} > 0.75$.

Ratchet transport from the ground state. We experimentally observe a SHR with matter waves using BECs of $5 \cdot 10^5$ ^{87}Rb atoms initially obtained in a hybrid trap setup [39]. The atoms are adiabatically loaded at time $T_0 = 0$ in the ground state $|\phi_0\rangle$ of the optical lattice potential

$$V(X,T) = -A(T)\frac{s}{2}E_{\mathrm{L}}\cos\left(\frac{2\pi X}{d} + \varphi(T)\right), \qquad (3)$$

with $A(T_0) = 1$ and $\varphi(T_0) = 0$ (we denote with capital X, P and T dimensional quantities). The optical lattice is produced by the superposition of two counterpropagating far-detuned laser beams of wavelength $\lambda = 1064$ nm. Before each experiment, we independently calibrate [40] the depth s of the lattice in units of the lattice energy scale $E_{\mathrm{L}} = h^2/2md^2$ (with $d = \lambda/2$ the lattice spacing, m the atomic mass and h Planck's constant). The driving amplitude of an acousto-optic modulator (AOM) placed before the splitting of the lattice beams controls $A(T)$, while the relative driving phase of two AOMs following the beams splitting controls $\varphi(T)$. The optical lattice potential (3), with the correlated modulation functions $A(T) = (1 + \varepsilon\cos(\omega T))$ and $\varphi(T) = -\varphi_0\sin(\omega T)$ where ω is the modulation angular frequency, yields the dimensionless gating Hamiltonian (1) for $\gamma = s(E_{\mathrm{L}}/\hbar\omega)^2$ and an effective reduced Planck constant $\hbar_{\mathrm{eff}} = 2E_{\mathrm{L}}/\hbar\omega$ [41].

The $1/\hbar_{\mathrm{eff}}$ range of Fig. 2 corresponds in practice to a lattice depth range $s \in [0.5, 14]$. A weak harmonic trapping with angular frequencies $(\Omega_X, \Omega_Y, \Omega_Z) = 2\pi \times (10.4, 66, 68)$ Hz remains present during experiments, but its impact is negligible over the short experimental times of up to ~ 500 µs in this work. In the subspace of null quasi-momentum, the BEC state along the x-axis is thus described by a superposition of plane waves

$$|\psi(T)\rangle = \sum_{\ell\in\mathbb{Z}} c_\ell(T)\,|\chi_\ell\rangle\,, \qquad (4)$$

with the coefficients $c_\ell(T) \in \mathbb{C}$, $\sum_\ell |c_\ell(T)|^2 = 1$ and $\langle X|\chi_\ell\rangle = e^{i\ell k_{\mathrm{L}} X}/\sqrt{d}$, where $k_{\mathrm{L}} = 2\pi/d$ is the lattice wavevector. Finally, we access at time T the BEC momentum distribution by absorption imaging following a 35 ms time-of-flight. We obtain the typical diffraction patterns of Fig. 1, from which we extract $|c_\ell(T)|^2$. The experimental transport (2) is then computed by sampling the average momentum $\langle\hat{P}\rangle_{\psi(T)}/\hbar k_{\mathrm{L}} = \sum_\ell \ell|c_\ell(T)|^2$ in the course of the ratchet modulation.

We first perform ratchet transport experiments with $|\phi_0\rangle$ as the initial state. We acquire 4 images per modulation period over 10 periods (as shown in Fig. 1 for the first period). Figure 3 shows, for two values of $1/\hbar_{\mathrm{eff}}$, the experimental evolution of the momentum distribution and the resulting integrated transport compared with numerical simulations of the same quantities from the integration of Schrödinger equation. The values of $1/\hbar_{\mathrm{eff}}$ in Fig. 3(a) and (b) correspond to those of Fig. 2(d) and (e) respectively. For Fig. 3(a), $|\phi_0\rangle$ is rather well projected onto $|\mathrm{F_{rat}}\rangle$ (Fig. 2(a,d)). We thus observe an almost periodic evolution of the momentum distribution, mainly carried by plane waves of positive momentum and resulting in a linear semiclassical ratchet transport over 10 lattice sites in 10 modulation periods (Fig. 3(c)). In the experiment of Fig. 3(b) however, as $|\phi_0\rangle$ has limited overlap with $|\mathrm{F_{rat}}\rangle$, which moreover extends over the chaotic sea (Fig. 2(e)), we observe a non-periodic evolution of the momentum distribution associated with a diffusion over the chaotic sea as seen from the increase of the momentum dispersion. This results in a non-linear evolu-

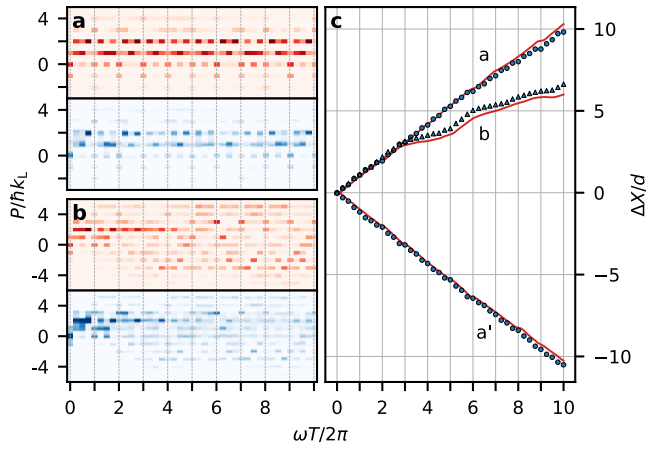

FIG. 3. **Transport of the ground state. (a)** Top: Numerical simulation of the momentum distribution during the modulation as a function of time for $1/\hbar_{\rm eff} \approx 1.27$ (corresponding to Fig. 2(d)). Bottom: Corresponding experimental integrated absorption images. **(b)** Same as (a) for $1/\hbar_{\rm eff} \approx 1.56$ (corresponding to Fig. 2(e)). **(c)** Expected numerical (solid red line) and experimental (blue markers) transport (see text) for data (a) and (b) as a function of time, and transport reversability (a') for $\varphi_0 \to -\varphi_0$ and $1/\hbar_{\rm eff} \approx 1.30$ (see text).

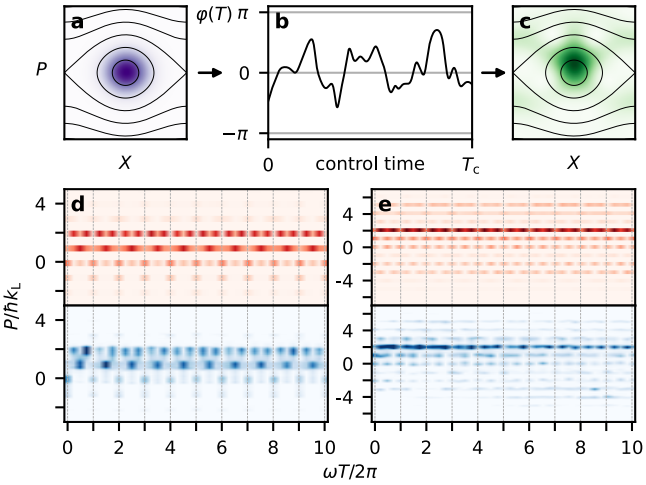

FIG. 4. **Transport of the ratcheting Floquet state prepared by QOC. (a-c)** Example of QOC for ratchet transport at $1/\hbar_{\rm eff} \approx 1.56$. **(a)** Husimi representation of $|\phi_0\rangle$ (purple) in the phase space of the static lattice (solid black lines). The color range for the Husimi function extends from zero to its maximum value. **(b)** Phase of the lattice along time to drive the system from $|\phi_0\rangle$ to $|\mathrm{F}_{\rm rat}\rangle$. **(c)** Same as (a) for the prepared state $|\psi_{\rm QOC}\rangle$. **(d)** Top: Numerical simulation of the momentum distribution during the modulation as a function of time for $1/\hbar_{\rm eff} \approx 1.27$ (corresponding to Fig. 2(d) and Fig. 3(a)). Bottom: Corresponding experimental integrated absorption images. **(e)** Same as (d) for $1/\hbar_{\rm eff} \approx 1.56$ (corresponding to panels (a-c) as well as Fig. 2(e) and Fig. 3(b)).

tion of the transport (Fig. 3(c)), in contrast to its classical counterpart. Interestingly, this non-classical behavior happens for a smaller value of $\hbar_{\rm eff}$, highlighting the quantum nature of the underlying mechanism of state mixing (see Supplemental Material).

A key feature of the ratchet effect is the ability to reverse the transport direction via adequate symmetries [3, 7]. In our gating system, this transport direction is imposed by the sign of the phase quadrature between the amplitude and phase modulations (Eq. (1)). The change $\varphi(t) = -\varphi_0 \sin(t) \to +\varphi_0 \sin(t)$ is thus expected to result in a reversed ratchet transport in the lattice. In Fig. 3(c), the integrated transport for $(\gamma, \varepsilon, \varphi_0) = (1.2, 0.3, -1.7)$ and a value of $\hbar_{\rm eff}$ similar to that of panel (a) is shown (with label (a')). We measure as expected a symmetric ratchet transport over -10 sites in 10 modulation periods. We get an overall excellent agreement between experiments and simulations.

Optimized loading through quantum optimal control. Even for values of $1/\hbar_{\rm eff}$ for which $\Delta x_{(0,2\pi)}(\mathrm{F}_{\rm rat}) \approx 2\pi$, semiclassical ratchet transport can be limited when working with $|\phi_0\rangle$ as the initial state (see *e.g.* Fig. 2(a,b,e)). To enhance this transport, we use, in a second set of experiments, the phase of the lattice φ as a control parameter to optimally prepare $|\mathrm{F}_{\rm rat}\rangle$ before applying the ratchet modulation. To that end, after determination of $|\mathrm{F}_{\rm rat}\rangle$, an optimal phase variation $\varphi(0 < T < T_c)$ in the lattice of fixed depth s is computed using a first-order gradient-ascent algorithm (detailed with its experimental implementation in previous works [42, 43]), to drive the BEC from $|\phi_0\rangle$ to $|\mathrm{F}_{\rm rat}\rangle$. We set in this work $T_c \approx 80\,\mu$s. The QOC algorithm converges to a control field that theoretically prepares a state $|\psi_{\rm QOC}\rangle$ with a fidelity of $|\langle \mathrm{F}_{\rm rat}|\psi_{\rm QOC}\rangle|^2 \geq 0.995$ [44]. We illustrate in Fig. 4(a-c) the QOC protocol of Floquet state preparation, with an optimized $\varphi(T)$ driving $|\phi_0\rangle$ to $|\mathrm{F}_{\rm rat}\rangle$ for a given value of $1/\hbar_{\rm eff}$ (corresponding to Fig. 2(e) and Fig. 3(b)). Figure 4(d,e) shows experimental results and numerical simulations for the same parameters as Fig. 3(a,b) respectively, with a preliminary QOC preparation applied. While the experiment of Fig. 3(a) already featured a clear linear quantum transport, Fig. 4(d) demonstrates how the QOC preparation of the ratcheting Floquet state enhances the periodicity of the momentum evolution. Comparing Fig. 4(e) with Fig. 3(b), the gain is even more spectacular. Interestingly, Fig. 4(e) display a broad momentum dispersion from the beginning of the modulation, which demonstrates the preparation of a ratcheting Floquet state partially extending over the chaotic sea as expected (see Fig. 2(e)).

Conclusion In this Letter, we have studied a spatial Hamiltonian ratchet effect exploiting regular trajectories in phase space to transport particles periodically at rest. We showed how such a SHR can be obtained classically within a gating ratchet. We then considered

quantum transport in the near semiclassical regime, for small but realistic values of the effective Planck constant $\hbar_{\rm eff}$, and discussed how quantum transport can be strongly affected by Floquet state mixing as $\hbar_{\rm eff}$ varies. We experimentally observed the SHR transport of matter waves with a BEC of ^{87}Rb in a modulated optical-lattice. For values of $\hbar_{\rm eff}$ coupling the ratcheting island with the chaotic sea, we witnessed how atoms loaded in the island evolve out of it through dynamical tunneling. Finally, we demonstrated how this effect can be mitigated through the use of state control methods such as QOC, to prepare the ratcheting Floquet state and thus enhance the periodicity of the dynamics.

Our modeling relies on an infinite lattice description, and is in good agreement with experimental data. Finite-size effects therefore have a limited impact on our experiments, which is due both to the extension of the BEC ($\approx$ 100 lattice sites) and to the fact that in the cases studied here the ratcheting Floquet state has a uniform group velocity in the vicinity of zero quasi-momentum (see Supplemental Material).

The regular ratchet effect we demonstrated constitutes a novel way to coherently transport matter wave in a periodic potential, alongside conveyor belt approaches [45–47]. Our results lend themselves to further investigations, such as the extension to higher dimensional modulated lattices, the investigation of the impact of interactions on the transport dynamics, or the use of optimal control to optimize the actual shape of the transporting state, in order *e.g.* to maximize its initial overlap with the ground state of the potential.

Aknowledgements We thank Gabriel Chatelain and Maxime Martinez for helpful discussions as well as Alexandre Dugelay for experimental support. This work was (partially) supported through the EUR Grant NanoX No. ANR-17-EURE-0009 in the framework of the "Programme d'Investissements d'Avenir" and research funding Grants No. ANR-17-CE30-0024 and ANR-22-CE47-0008. N.D. and F.A. acknowledge support from Région Occitanie and Université Toulouse III-Paul Sabatier. N.D. acknowledges ERC Grant LATIS for support in Brussels.

SUPPLEMENTAL MATERIAL: AVOIDED CROSSINGS AND STATE COUPLING

In Fig. 5 we illustrate the mechanism of Floquet state mixing under the variation of $1/\hbar_{\rm eff}$, responsible for the non-monotonous variations of the loading and transport of the ratcheting Floquet state (Fig. 2(a,b)).

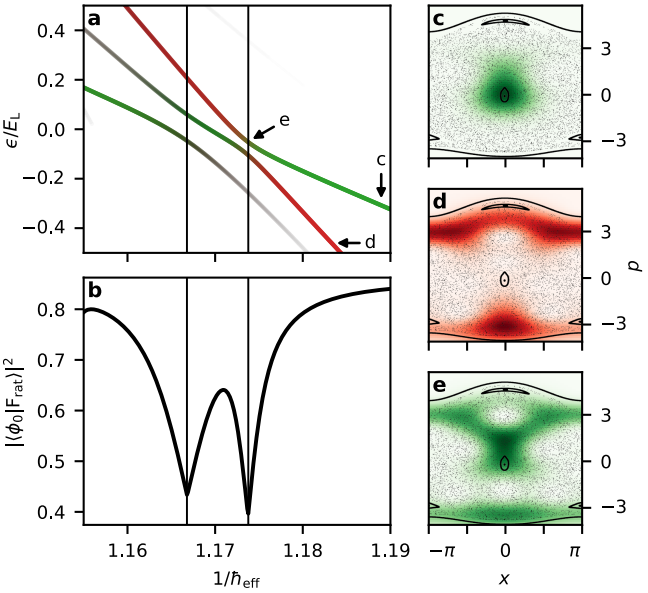

FIG. 5. **Avoided crossings and state coupling.** **(a)** Part of the Floquet quasi-energy spectrum as a function of $1/\hbar_{\rm eff}$ for the modulated Hamiltonian (1) with parameters $(\gamma, \varepsilon_0, \varphi_0) = (1.2, 0.3, 1.7)$. The quasi-energy ϵ is plotted reduced by the characteristic lattice energy $E_{\rm L}$ (see main). The Floquet states associated with the quasi-energy marked by the letters (c) and (d) are identified near $1/\hbar_{\rm eff} = 1.19$ from their overlap with a coherent state centered in $(x, p) = (0, 0)$ and associated to green and red colors. The whole spectrum is then colored depending on the overlaps with these states. In practice the ratcheting Floquet state $|{\rm F_{rat}}\rangle$ corresponds to the most green quasi-energy across the spectrum. **(b)** Overlap between $|{\rm F_{rat}}\rangle$ and the ground state $|\phi_0\rangle$ of the static potential (*i.e.* magnified excerpt from Fig. 2(a)). The black vertical lines in (a,b) mark the position of the two avoided crossings seen in (a) corresponding to the two drops in ground state overlap seen in (b). **(c-e)** Stroboscopic phase portraits and Husimi representations of the three states associated with the quasi-energies identified in (a).

SUPPLEMENTAL MATERIAL: FLOQUET SPECTRA OF RATCHET SYSTEMS

For the three values of $1/\hbar_{\rm eff}$ considered on Fig. 2, we represent a part of their Floquet spectrum on Fig. 6. More specifically, we represent for each quasi-momentum q in the Brillouin zone, the quasi-energies ϵ of the periodic Hamiltonian (1), with the weight of the drawn line denoting the weight of the projection of a given Floquet state at quasi-momentum q on the corresponding state in the lowest band of the static lattice $|\phi_q\rangle$. The ratcheting state $|{\rm F_{rat}}\rangle$ (see main text) corresponds therefore to the dominant quasi-energy level at $q = 0$. Its transport over one period (see main text) is related to the time-averaged group velocity that can be extracted from the spectrum

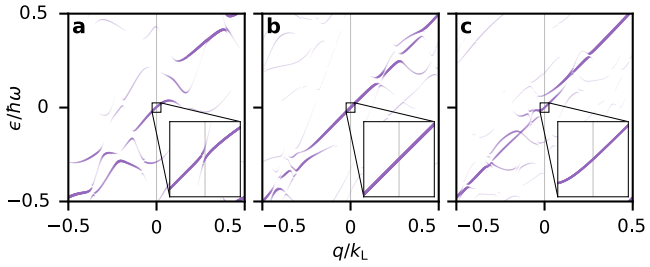

FIG. 6. Floquet spectra for the modulation parameters of Fig. 2(c,d,e) (panels (a,b,c) respectively). On each spectrum, the quasi-energies ϵ are drawn over a Brillouin zone ($|q| < k_L/2$ and $|\epsilon| < \hbar\omega/2$) and weighted by the projection of the Floquet state onto the corresponding ground state of the static lattice $|\phi_q\rangle$ at the same quasimomentum q. The ratcheting state $|F_{rat}\rangle$ corresponds therefore to the dominant quasi-energy level at $q = 0$. On each panel, an inset provides a zoom on the central region of width $\Delta q/k_L = 0.05$. In the dimensionless units chosen, a transport of one lattice site d per period of modulation $2\pi/\omega$ corresponds to a local slope of 1.

(in dimensionless units):

$$\overline{v}_g = \frac{2\pi}{\omega d}\frac{1}{\hbar}\frac{\partial \epsilon}{\partial q} = \frac{\Delta x_{(0,2\pi)}}{2\pi}.$$

The spectra in Fig. 6 further illustrate the characteristics of ratcheting states presented in Fig. 2. For the state Fig. 2(c), the spectrum Fig. 6(a) demonstrates that the sharp change in transport, as well as projection on the ground state, is mostly due to a very narrow avoided crossing in quasi-momentum near $q = 0$. For the state Fig. 2(e), the spectrum Fig. 6(c) shows that the ratcheting state belongs to an energy band with slope ≈ 1, therefore has an average transport $\Delta x_{(0,2\pi)}(F_{rat}) \approx 2\pi$. However the ground state of the lattice projects on several Floquet states at $q = 0$ (with different transport properties), which explains the poor transport from ground state loading observed in Fig. 3(b,c). Finally in the case of Fig. 2(d), the good loading of the ratcheting state from the ground state is also evidenced by the spectrum Fig. 6(b), where $|\phi_0\rangle$ projects almost solely on $|F_{rat}\rangle$, and the slope of the quasi-energy band is equal to 1. The fact that this remains true for a neighborhood of $q = 0$ implies that a finite-size wavepacket should then propagate non-dispersively across lattice sites [23].

[1] S. Flach, O. Yevtushenko, and Y. Zolotaryuk, Directed Current due to Broken Time-Space Symmetry, Phys. Rev. Lett. **84**, 2358 (2000).

[2] S. Denisov, S. Flach, A. A. Ovchinnikov, O. Yevtushenko, and Y. Zolotaryuk, Broken space-time symmetries and mechanisms of rectification of ac fields by nonlinear (non)adiabatic response, Phys. Rev. E **66**, 041104 (2002).

[3] S. Denisov, S. Flach, and P. Hänggi, Tunable transport with broken space–time symmetries, Physics Reports **538**, 77 (2014).

[4] P. Hänggi and F. Marchesoni, Introduction: 100 years of Brownian motion, Chaos: An Interdisciplinary Journal of Nonlinear Science **15**, 026101 (2005).

[5] J. Rousselet, L. Salome, A. Ajdari, and J. Prost, Directional motion of brownian particles induced by a periodic asymmetric potential, Nature **370**, 446 (1994).

[6] R. D. Astumian and P. Hänggi, Brownian motors, Physics Today **55**, 33 (2002).

[7] P. Hänggi and F. Marchesoni, Artificial Brownian motors: Controlling transport on the nanoscale, Rev. Mod. Phys. **81**, 387 (2009).

[8] F. Jülicher, A. Ajdari, and J. Prost, Modeling molecular motors, Rev. Mod. Phys. **69**, 1269 (1997).

[9] D. Chowdhury, A. Schadschneider, and K. Nishinari, Traffic phenomena in biology: From molecular motors to organisms, in *Traffic and Granular Flow'05*, edited by A. Schadschneider, T. Pöschel, R. Kühne, M. Schreckenberg, and D. E. Wolf (Springer Berlin Heidelberg, Berlin, Heidelberg, 2007) pp. 223–238.

[10] M. Nishiyama, H. Higuchi, and T. Yanagida, Chemomechanical coupling of the forward and backward steps of single kinesin molecules, Nature Cell Biology **4**, 790 (2002).

[11] P. Reimann, Brownian motors: noisy transport far from equilibrium, Physics Reports **361**, 57 (2002).

[12] C. Mennerat-Robilliard, D. Lucas, S. Guibal, J. Tabosa, C. Jurczak, J.-Y. Courtois, and G. Grynberg, Ratchet for Cold Rubidium Atoms: The Asymmetric Optical Lattice, Phys. Rev. Lett. **82**, 851 (1999).

[13] P. Jung, J. G. Kissner, and P. Hänggi, Regular and Chaotic Transport in Asymmetric Periodic Potentials: Inertia Ratchets, Phys. Rev. Lett. **76**, 3436 (1996).

[14] M. Schiavoni, L. Sanchez-Palencia, F. Renzoni, and G. Grynberg, Phase Control of Directed Diffusion in a Symmetric Optical Lattice, Phys. Rev. Lett. **90**, 094101 (2003).

[15] G. G. Carlo, G. Benenti, G. Casati, and D. L. Shepelyansky, Quantum Ratchets in Dissipative Chaotic Systems, Phys. Rev. Lett. **94**, 164101 (2005).

[16] L. Wang, G. Benenti, G. Casati, and B. Li, Ratchet Effect and the Transporting Islands in the Chaotic Sea, Phys. Rev. Lett. **99**, 244101 (2007).

[17] I. Dana, V. Ramareddy, I. Talukdar, and G. S. Summy, Experimental Realization of Quantum-Resonance Ratchets at Arbitrary Quasimomenta, Phys. Rev. Lett. **100**, 024103 (2008).

[18] R. Gommers, V. Lebedev, M. Brown, and F. Renzoni, Gating Ratchet for Cold Atoms, Phys. Rev. Lett. **100**, 040603 (2008).

[19] S. Denisov, S. Kohler, and P. Hänggi, Underdamped quantum ratchets, EPL (Europhysics Letters) **85**, 40003 (2009).

[20] H. Schanz, M.-F. Otto, R. Ketzmerick, and T. Dittrich, Classical and Quantum Hamiltonian Ratchets, Phys. Rev. Lett. **87**, 070601 (2001).

[21] S. Denisov, L. Morales-Molina, S. Flach, and P. Hänggi, Periodically driven quantum ratchets: Symmetries and resonances, Phys. Rev. A **75**, 063424 (2007).

[22] T. Salger, S. Kling, T. Hecking, C. Geckeler, L. Morales-Molina, and M. Weitz, Directed Transport of Atoms in a Hamiltonian Quantum Ratchet, Science **326**, 1241

(2009).
[23] F. Zhan, S. Denisov, A. V. Ponomarev, and P. Hänggi, Quantum ratchet transport with minimal dispersion rate, Physical Review A **84**, 043617 (2011).
[24] R. Citro and M. Aidelsburger, Thouless pumping and topology, Nature Reviews Physics **5**, 87 (2023).
[25] J. Gong and P. Brumer, Directed anomalous diffusion without a biased field: A ratchet accelerator, Phys. Rev. E **70**, 016202 (2004).
[26] D. H. White, S. K. Ruddell, and M. D. Hoogerland, Experimental realization of a quantum ratchet through phase modulation, Phys. Rev. A **88**, 063603 (2013).
[27] C. Hainaut, A. Rançon, J.-F. Clément, J. C. Garreau, P. Szriftgiser, R. Chicireanu, and D. Delande, Ratchet effect in the quantum kicked rotor and its destruction by dynamical localization, Phys. Rev. A **97**, 061601 (2018).
[28] T. Dittrich, R. Ketzmerick, M.-F. Otto, and H. Schanz, Classical and quantum transport in deterministic hamiltonian ratchets, Annalen der Physik **512**, 755 (2000).
[29] M. Borromeo and F. Marchesoni, Noise-assisted transport on symmetric periodic substrates, Chaos: An Interdisciplinary Journal of Nonlinear Science **15**, 026110 (2005).
[30] C. Grossert, M. Leder, S. Denisov, P. Hänggi, and M. Weitz, Experimental control of transport resonances in a coherent quantum rocking ratchet, Nature Communications **7**, 10440 (2016).
[31] S. Tomsovic and D. Ullmo, Chaos-assisted tunneling, Phys. Rev. E **50**, 145 (1994).
[32] M. Arnal, G. Chatelain, M. Martinez, N. Dupont, O. Giraud, D. Ullmo, B. Georgeot, G. Lemarié, J. Billy, and D. Guéry-Odelin, Chaos-assisted tunneling resonances in a synthetic Floquet superlattice, Science Advances **6**, eabc4886 (2020).
[33] S. Keshavamurthy and P. Schlagheck, eds., *Dynamical Tunneling: Theory and Experiment* (CRC Press, 2011).
[34] U. Boscain, M. Sigalotti, and D. Sugny, Introduction to the Pontryagin Maximum Principle for Quantum Optimal Control, PRX Quantum **2**, 030203 (2021).
[35] C. P. Koch, U. Boscain, T. Calarco, G. Dirr, S. Filipp, S. J. Glaser, R. Kosloff, S. Montangero, T. Schulte-Herbrüggen, D. Sugny, and F. K. Wilhelm, Quantum optimal control in quantum technologies. Strategic report on current status, visions and goals for research in Europe, EPJ Quantum Technology **9**, 19 (2022).
[36] N. Dupont, *Control and transport of matter waves in an optical lattice*, Ph.D. thesis, Université Toulouse 3 - Paul Sabatier (2022).
[37] M. V. Berry and M. Robnik, Semiclassical level spacings when regular and chaotic orbits coexist, Journal of Physics A: Mathematical and General **17**, 2413 (1984).
[38] O. Bohigas, S. Tomsovic, and D. Ullmo, Manifestations of classical phase space structures in quantum mechanics, Physics Reports **223**, 43 (1993).
[39] A. Fortun, C. Cabrera-Gutiérrez, G. Condon, E. Michon, J. Billy, and D. Guéry-Odelin, Direct Tunneling Delay Time Measurement in an Optical Lattice, Phys. Rev. Lett. **117**, 010401 (2016).
[40] C. Cabrera-Gutiérrez, E. Michon, V. Brunaud, T. Kawalec, A. Fortun, M. Arnal, J. Billy, and D. Guéry-Odelin, Robust calibration of an optical-lattice depth based on a phase shift, Phys. Rev. A **97**, 043617 (2018).
[41] Having $\gamma = s(E_{\mathrm{L}}/\hbar\omega)^2$ and $\hbar_{\mathrm{eff}} = 4\pi^2\hbar/m\omega d^2$, $\hbar_{\mathrm{eff}}$ is varied without altering the classical dynamics by adjusting the lattice depth $s = 4\gamma/\hbar_{\mathrm{eff}}^2$.
[42] N. Dupont, G. Chatelain, L. Gabardos, M. Arnal, J. Billy, B. Peaudecerf, D. Sugny, and D. Guéry-Odelin, Quantum State Control of a Bose-Einstein Condensate in an Optical Lattice, PRX Quantum **2**, 040303 (2021).
[43] N. Dupont, F. Arrouas, L. Gabardos, N. Ombredane, J. Billy, B. Peaudecerf, D. Sugny, and D. Guéry-Odelin, Phase-space distributions of Bose–Einstein condensates in an optical lattice: optimal shaping and reconstruction, New Journal of Physics **25**, 013012 (2023).
[44] This fidelity figure is set as a convergence condition on the iterative QOC algorithm [42].
[45] D. Schrader, S. Kuhr, W. Alt, M. Müller, V. Gomer, and D. Meschede, An optical conveyor belt for single neutral atoms, Applied Physics B **73**, 819 (2001).
[46] S. H. Hauck, G. Alber, and V. M. Stojanović, Single-atom transport in optical conveyor belts: Enhanced shortcuts-to-adiabaticity approach, Physical Review A **104**, 053110 (2021).
[47] T. Klostermann, C. R. Cabrera, H. von Raven, J. F. Wienand, C. Schweizer, I. Bloch, and M. Aidelsburger, Fast long-distance transport of cold cesium atoms, Physical Review A **105**, 043319 (2022).